Environ Sci Pollut Res (2014) 21:1582–1591
DOI 10.1007/s11356-013-2059-1

RESEARCH ARTICLE

Photocatalytic discoloration of Methyl Orange by anatase/schorl composite: optimization using response surface method

Huan-Yan Xu · Wei-Chao Liu · Jian Shi · Hang Zhao · Shu-Yan Qi

Received: 27 June 2013 / Accepted: 1 August 2013 / Published online: 14 August 2013
© Springer-Verlag Berlin Heidelberg 2013

Abstract The anatase/schorl composites were prepared and employed for the photocatalytic discoloration of an azo dye, Methyl Orange (MO). X-ray diffraction results indicated that TiO_2 existed in the form of anatase phase and no diffraction peaks of schorl could be observed for all the composite samples. Scanning electron micrographs showed that the particles of anatase were well deposited and dispersed on the surface of schorl. Photocatalytic experiments revealed that the anatase/schorl composites exhibited higher photocatalytic activity for MO discoloration than pure TiO_2 and more than 90 % discoloration ratio could be obtained within 60 min UV irradiation when the sample containing 3 wt.% of schorl as TiO_2 support was used. Then, the central composite design (CCD) under the response surface methodology (RSM) was employed for the experiment design and process optimization. The significance of a second-order polynomial model for predicting the optimal values of MO discoloration was evaluated by the analysis of variance (ANOVA) and 3D response surface plots for the interactions between two variables were constructed. Based on the model prediction, the optimum conditions for the photocatalytic discoloration of MO by TiO_2/schorl composite were determined to be 15×10^{-3} mM MO initial concentration, 2.7 g/l photocatalyst dosage, solution pH 6.6 and 43 min reaction time, with a maximum MO discoloration ratio of 98.6 %. Finally, a discoloration ratio of 94.3 % was achieved for the real sample under the optimum conditions, which was very close to the predicted value, implying that RSM is a powerful and satisfactory strategy for the process optimization.

Keywords Anatase · Schorl · Methyl Orange · Photocatalysis · Process optimization · Response surface methodology

Introduction

Effluent containing reactive dyes from textile dyeing and finishing industries is a significant source of environmental pollution (Xu et al. 2013). Hence, the discharge of wastewater from a textile industry is a subject of great concern with regard to environmental safety and needs proper treatment to reduce the dye concentration below the permissible limit (Mohanta et al. 2013). Azo dyes are the largest category of synthetic dyes with an estimated share of about 70 % and widely used in textile, leather tanning, printing, and photography. They contain one or more azo bonds (—N=N—) as chromophore group in association with aromatic structures containing functional groups such as −OH and $-SO_3H$ (Ramírez et al. 2013). Azo dyes are recalcitrant to microbial biodegradation and are not easily degraded in traditional wastewater treatment processes (Zhang et al. 2013a), due to their complex chemical structures and synthetic origins (Chen et al. 2011). Many different technological methods, such as coagulation, flocculation, adsorption, membrane filtration, and advanced oxidation processes, have been employed for the treatment of azo dyes-containing wastewater. However, these methods suffered some shortcomings such as sludge generation, adsorbent regeneration, membrane fouling, high treatment costs, and potential formation of highly toxic by-products (Ong et al. 2013; Zhang et al. 2013a). During the past decade, the application of photocatalysis for wastewater and air purification from organic contaminants has attracted more and more attentions. Numerous studies have proved that TiO_2 (a semiconductor with a wide band gap 3.2 eV) and some other composite systems, based on modified TiO_2, are very efficient and promising photocatalysts (Eliyas et al. 2013).

Responsible editor: Philippe Garrigues

H.-Y. Xu (✉) · W.-C. Liu · J. Shi · H. Zhao · S.-Y. Qi
School of Materials Science and Engineering, Harbin University of Science and Technology, Harbin 150040, China
e-mail: xhy7587@yahoo.com.cn

Among various materials used as semiconductors, titanium dioxide (TiO_2) has been widely used for a broad range of applications because it is cheap, non-toxic, very active and stable in chemical reactions (Baek et al. 2013a). When a photon of light with sufficient energy ($E \geq E_{bg}$) strikes a TiO_2 particle, an electron (e^-) can be excited from the valence band to conduction band and a hole (h^+) be left in the valence band. h^+ and e^- can either recombine or migrate to the surface of TiO_2 particle where they can react with other species at the interface. The holes can directly oxidize organic species adsorbed onto the TiO_2 particle or can give rise to hydroxyl radicals (•OH) by reacting with water or OH^-. These highly reactive hydroxyl radicals then attack organic compounds present at or near the surface (Coleman et al. 2005). However, the expensive separation of suspensions of nano-sized TiO_2 powders from the solution is an obstacle to its utilization in large-scale photocatalysis (Eliyas et al. 2013). More recently, TiO_2 powders have been used after deposition onto supports in order to overcome problems associated with separation (and recovery) of the catalyst particles from the liquid phase (Petrella et al. 2013). Furthermore, the deposition of TiO_2 particles onto supports' surface under mild conditions is a promising method to resolve the agglomeration problem of TiO_2 (Papoulis et al. 2013). Many authors have been working on the immobilization of TiO_2 powder on various supports such as Al_2O_3 (Huang et al. 2013; Sedneva et al. 2013), SiO_2 (Dong et al. 2012; Harraz et al. 2013), clays (Blain et al. 2012; Kibanova et al. 2012; Zendehzaban et al. 2013), zeolites (Kamegawa et al. 2013; Mohamed and Baeissa 2013; Torkian et al. 2013; Zhang et al. 2013b), synthetic carbon (Lin et al. 2013; Wei et al. 2013), activated carbon (Li and Liu 2012; Yoon et al. 2012; Baek et al. 2013b), carbon nanotube (Da Dalt et al. 2013; Juang et al. 2013; Zhao et al. 2013), and graphene (Li et al. 2013; Morales-Torres et al. 2013; Wang et al. 2013). Compared with the pure sample, TiO_2 loaded onto the supports exhibited several advantages: (1) increase in specific surface area, (2) enhancement of the adsorption capacity, and (3) increase in the photocatalytic activity (Eliyas et al. 2013). On the other hand, external electric field has been applied to restrain the recombination of the electron–hole pairs to improve the photocatalytic activity of TiO_2. This process was described as a photo-electro-catalytic process (Xie et al. 2005) whose efficiency was much higher than that of the single photocatalytic process (Su et al. 2008). Schorl is one kind of minerals of the tourmaline groups. It has been confirmed that the spontaneous (or permanent) electrostatic poles exist on the surface of the tourmaline crystals at room temperature (Nakamura and Kubo 1992), and this property encouraged us to be the pioneers for the application of schorl as a TiO_2 support (Xu et al. 2010). The results indicated the photocatalytic activity of TiO_2/schorl composite for acid fuchsine (AF) discoloration was higher than that of pure TiO_2. The AF discoloration ratio approached 100 % after 12 h under UV irradiation and the reaction process followed pseudo-first-order kinetics, discussed by the Langmuir–Hinshelwood model. Subsequently, Bian et al. (2013) discussed in detail the photocatalytic model for the degradation of 2,4-dichlorophenoxyacetic acid (2,4-D) using the TiO_2/tourmaline composite as the catalyst. However, to the best of our knowledge, the process optimization about this system has not been involved up to now.

Response surface methodology (RSM) with a central composite design (CCD) is a powerful experiment design tool that has been widely used to optimize and evaluate the performance of multivariable systems. It can overcome the limitation of one-factor-at-a-time approach by collection of mathematical and statistical techniques (Zhang et al. 2013a). Under this methodology, it is possible to identify optimal conditions while minimizing the number of experiments required for a selected response (Rosales et al. 2012). Optimal reaction conditions in terms of cost and treatment efficiency are required to be established to improve the overall process performance. Two approaches are usually adopted for process optimization: one-factor-at-a-time and two-level-factorial-design. The one-factor-at-a-time optimization technique of changing one variable at a time to study the effects of variables on the response has been widely used in process optimization, but it is time consuming and expensive, particularly for multivariable systems, without showing the effect of interactions between different factors. Two-level-factorial-design can be used to overcome the inter-variable interaction, which is a statistics based method that involves simultaneous adjustment of experimental factors at only two levels. Although two-level-factorial-design cannot investigate fully a wide range in the factor space, it can indicate major trends (Umar et al. 2010). The experimental design and optimization by RSM involved the following steps: (1) the implementation of the statistically designed experiments; (2) the estimation of the coefficients of a mathematical model using regression analysis technique; (3) the prediction of the response; and (4) the verification of the adequacy of the model (Gilpavas et al. 2012). In this present study, CCD under RSM was employed for the process optimization of the photocatalytic discoloration of an azo dye, Methyl Orange (MO) using TiO_2/schorl composite as the catalyst.

Materials and methods

Materials

Powdered particles of schorl, with the size range of <64 μm, were purchased from Wuhua-Tianbao Mining Resources Co. Ltd. (Inner Mongolia, China). An azo dye, MO, was selected for this study as the target pollutant; it was used without any additional purification and its molecular structure and related information are shown in Fig. 1. All other chemicals and

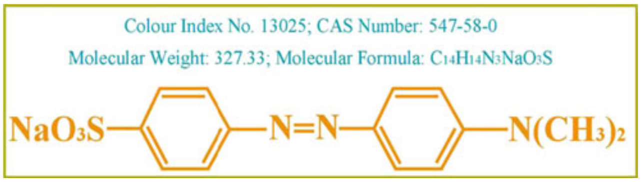

Fig. 1 Molecular structure and related information of MO

reagents were of analytical grade and also used without further purification. All solutions were prepared in deionized water. The preparation procedure of the composite photocatalysts has been introduced in detail elsewhere (Xu et al. 2010). Briefly, after pretreatment with HCl (1 M) at room temperature for 24 h, several grams of schorl powder was added to a mixture composed by tetrabutyl orthotitanate ($Ti(OC_4H_9)_4$), diethanol amine ($NH(OC_2H_5)_2$), ethanol (C_2H_5OH) and deionized water in a molar ratio of 1:1:30:1. After 1 h of stirring, deionized water was added, and then a translucent sol was obtained. Subsequently, the solvent was removed by filtration and the resultant solid was dried at 100 °C for 24 h. Finally, the prepared sample was sintered at 550 °C for 2.5 h. After ground, the powdered sample of TiO_2/schorl composite catalyst was obtained. In this study, the composite photocatalysts with different schorl contents of 1, 2, 3, 4, and 6 wt.% were prepared at 550 °C, labeled as TS1, TS2, TS3, TS4, and TS6, respectively. For comparison, the pure TiO_2 sample was also prepared using the same procedure except for the addition of schorl.

Characterization

The crystalline phases of the raw schorl, pure TiO_2 and TiO_2/schorl composite were determined by X-ray diffraction (XRD). Measurements were carried out on a D/MAX-3B X-ray diffractometer with Cu-Kα radiation (λ=1.5418 Å) at 30 mA and 40 kV, over the 2θ range of 10–80°. The crystal morphologies were observed using a scanning electron microscope (SEM). Measurements were made on a FEISirion200 SEM instrument using a digital imaging process. The surface area of composite photocatalysts was obtained from nitrogen adsorption–desorption data and measured using a ST-08 surface area analyzer at liquid nitrogen temperature.

Photocatalytic experiments

The photocatalytic discoloration of MO was conducted in a 200-ml glass reactor at room temperature. The 30-W ZSZ15-40 UV lamp, with predominant UV radiation at a wavelength of 253.7 nm, was located at about 15 cm above the solution. Generally, 100 ml of MO solution and certain gram of the photocatalyst were placed in the reactor before irradiation. At regular time intervals of irradiation, 2 ml of the samples was collected from the reactor for measurements of MO concentrations, using a 721- type UV–vis spectrophotometer at the wavelength of 482 nm. The discoloration ratio was calculated as follows: $D(\%)=(C_0-C_t)/C_0\times100$, where C_0 is the initial concentration of the MO wastewater and C_t is the concentration at irradiation time t. In order to evaluate the adsorption of MO on the photocatalysts, experiments were performed under the same condition but without UV irradiation and the adsorbed MO concentration was deducted. Furthermore, random tests were done for different experimental conditions to check the reproducibility of the obtained results.

Experimental design, analysis and optimization

Four factors, in this work, were selected as independent variables. They were the initial MO concentration (10^{-3} mM), reaction time (min), catalyst dosage (g/l), and solution pH, assigned with the following notations X_1, X_2, X_3 and X_4, respectively. At the same time, MO discoloration ratio (%) was chosen as the output variable (response, Y). The experimental design, mathematical modeling and optimization were performed with the Design Expert 8.0.5.0 software (Stat-Ease, Inc.) in this work. For statistical calculations, the variables X_i were coded as x_i according to the following equation (Fathinia et al. 2010; Gilpavas et al. 2012):

$$x_i = \frac{X_i - X_0}{\delta X}, \tag{1}$$

where x_i is the code value, X_i is the uncoded value, X_0 is the value of X_i at the center point and δX presents the step change. The experimental ranges and the levels of the independent variables for MO discoloration are listed in Table 1. The preliminary experiments were conducted to determine the ranges of the independent variables. A second-order regression model was employed to analyze and fit the responses to

Table 1 The variables, their codes and real experimental values used in CCD

Variables	Coded levels				
	−2	−1	0	1	2
MO initial concentration (10^{-3} mM), X_1	3	9	15	21	27
Reaction time (min), X_2	10	20	30	40	50
Catalyst dosage (g/l), X_3	1	2	3	4	5
Solution pH, X_4	3	5	7	9	11

the independent variables, shown in Eq. 2 (Arslan-Alaton et al. 2010; Khataee et al. 2012; Lak et al. 2012).

$$Y = \beta_0 + \sum_{i=1}^{k} \beta_i X_i + \sum_{i=1}^{k} \beta_{ii} X_i^2 + \sum_i \sum_j \beta_{ij} X_i X_j, \qquad (2)$$

where Y is response (MO discoloration ratio); X_i and X_j are the input variables that influence the response (Y); β_0 is an intercept constant; β_i is the first-order regression coefficient; β_{ii} is the second-order regression coefficient representing quadratic effect of factor i; and β_{ij} is the coefficient of interaction between factors i and j. Analysis of variance (ANOVA) was used to determine the significance of model and regression coefficients. The quality and prediction capacity of the polynomial equation was judged by the determination coefficient (R^2) (Gilpavas et al. 2012; Khataee et al. 2012). Otherwise, it should be mentioned that all experiments were carried out in duplicate and the average of the discoloration ratio was taken as the response. The standard deviation (SD) was less than 3 % (Rosales et al. 2012).

Results and discussion

Characterization of photocatalysts

The XRD patterns of schorl, TiO_2 and TiO_2/schorl composites are illustrated in Fig. 2, where it can be seen that the parent sample exhibits a typical trigonal structure of schorl, corresponding to JCPDS 22–469; and six distinctive diffraction peaks of TiO_2/schorl composites locate at 25.37°, 37.84°, 48.17°, 53.97°, 55.35° and 62.23°, corresponding to the crystal planes of (101), (004), (200), (105), (211), and (204) of the anatase phase of TiO_2 (JCPDS 78–2486), respectively. These results indicated that (1) TiO_2 existed in the form of anatase phase and no rutile phase could be found in all the composite samples, which would facilitate the photocatalytic reaction of the composite catalysts due to higher photocatalytic activity of anatase than that of rutile (Zhou et al. 2005); and (2) no XRD diffraction peaks of schorl could be observed for the composite samples, which might be attributed to the fact that the content of schorl was so low that it cloud not be detected by XRD. Even for 10 wt.% tourmaline mineral loaded onto TiO_2, it could not be detected by XRD as well (Song and Kang 2008).

The surface morphologies of the pure TiO_2 and composite samples were observed by SEM, and Fig. 3 shows representative SEM micrographs. It can be clearly found from the inset in Fig. 3, that the pure TiO_2 particles exhibit irregular shapes and they desultorily aggregate together. However, with respect to the composite samples, the particles of TiO_2 were well deposited and dispersed on the surface of schorl. The anchoring of TiO_2 particles on the surface of schorl in the composite were mainly attributed to the strong electrostatic adsorption by the electrostatic field on the schorl surface (Xu et al. 2010). Furthermore, the surface area of TS1, TS2, TS3, TS4, and TS6 was determined as 34.17, 37.58, 42.26, 54.13 and 60.05 g/m², respectively.

Preliminary experiments

The preliminary experiments were carried out to choose the best content of schorl in the composite catalysts with the highest photocatalytic activity and estimate the value ranges of the independent variables in RSM design. Keeping all other experimental parameters constant, the composite catalysts containing different wt.% of schorl as TiO_2 supports were

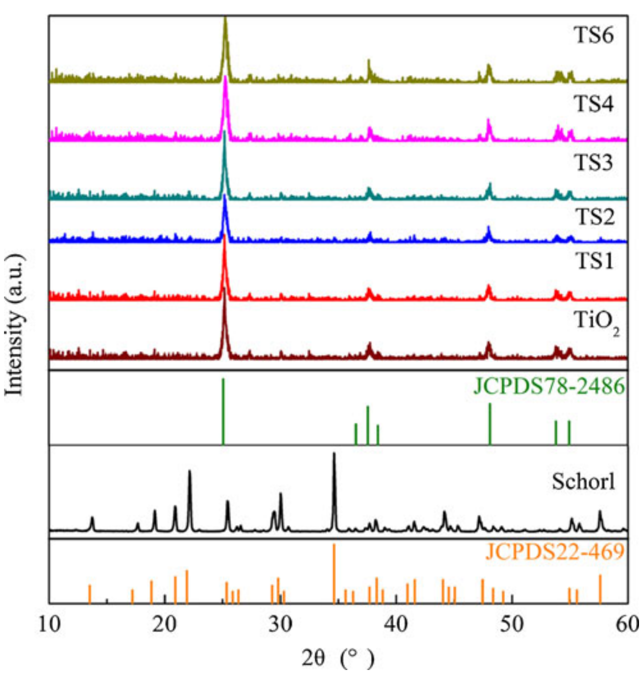

Fig. 2 XRD patterns of schorl, TiO_2 and TiO_2/schorl composites

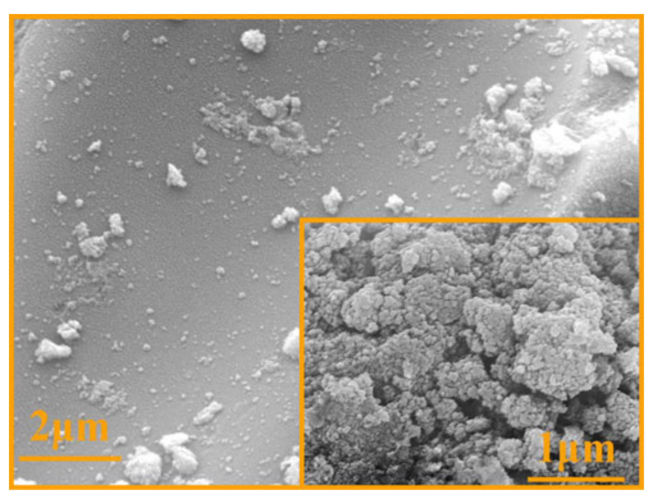

Fig. 3 SEM micrographs of composite TS3 and pure TiO_2 (*inset*)

employed to understand their influences on MO discoloration, as depicted in Fig. 4. The data clearly indicate that the MO discoloration ratio by TiO_2/schorl composite catalyst is much higher than that by the pure TiO_2, which implies that schorl can improve the photocatalytic activity of TiO_2. When the pure TiO_2 was used as photocatalyst, only 45 % MO could be discolored within 60 min irradiation, whereas more than 90 % MO discoloration ratio could be obtained in the same reaction time for TS3 catalyst. It is generally accepted that adsorption is critical in heterogeneous photocatalytic oxidation processes. In the dark adsorption experiments, the MO discoloration ratio after 1 h adsorption by TiO_2, TS1, TS2, TS3, TS4, and TS6 was observed to be 10.27, 11.84, 12.53, 13.22, 18.39 and 20.61 %, respectively, clearly indicating that, besides photocatalysis, adsorption also contributed to MO discoloration and the difference in the adsorption ratio was mainly caused by the surface area of the photocatalysts. So, the MO discoloration in this system was related to a synergistic effect of adsorption and photocatalysis. Furthermore, in this study, the optimum photocatalyst for the photocatalytic discoloration of MO was found to be TS3, which suggested that 3 wt.% was the preferable content of schorl in the composite photocatalyst for MO discoloration. Furthermore, the non-linear relationship between discoloration or removal ratios and support contents has been observed and discussed in many other studies (Blain et al. 2012; Chen et al. 2012; Zhang et al. 2013b; Zhao et al. 2013). Similar results have also been found in the decomposition of 2-chlorophenol by tourmaline loaded on TiO_2 (Song and Kang 2008) and the degradation of MO by SiO_2/TiO_2 doping with tourmaline (Meng et al. 2006). In this study, possible reasons put forward to interpret this phenomenon were that, on one hand, more than 3 wt.% of schorl in the composite catalyst might make the electrostatic field on the surface of schorl adsorb or disturb each other, as a whole, resulting in the reduction of the electrostatic strength; on the other hand, less than 3 wt.% of schorl in the composite catalyst might make relatively less amounts of 'electrostatic poles', which could reduce chances for the photogenerated electron migrating from TiO_2 to the interface of TiO_2/schorl, leading to the increase in recombination of the electrons and holes (Xu et al. 2010). So, 3 wt.% of schorl was determined to be the best content in the composite photocatalyst for the rapid transfer of the photogenerated electrons from TiO_2 semiconductor to the interface of TiO_2/schorl and tight adsorption of the electrons on the anode of schorl. Consequently, TS3 was chosen for the process optimization. In addition, based on these results, the value ranges of the independent variables in RSM design were determined and listed in Table 1.

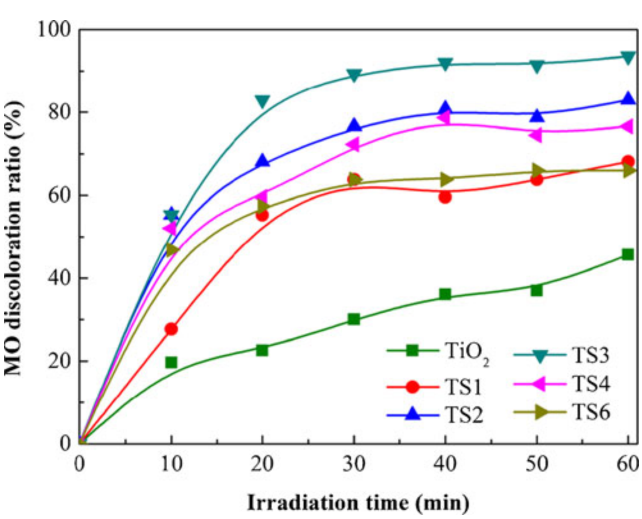

Fig. 4 Photocatalytic discoloration of MO over TiO_2/schorl composite catalyst containing different schorl contents at room temperature, pH=7, MO initial concentration=15×10^{-3} mM, and catalyst dosage=3 g/l

Table 2 Experimental design and response based on experimental runs proposed by CCD under RSM

Run	Variables				MO discoloration ratio (%)		Residual
	X_1	X_2	X_3	X_4	Eperimental	Predicted	
1	−1	−1	−1	−1	63.7	64.43	−0.73
2	1	−1	−1	−1	34.1	34.00	0.10
3	−1	1	−1	−1	79.2	81.55	−2.35
4	1	1	−1	−1	40.2	42.02	−1.82
5	−1	−1	1	−1	52.4	53.97	−1.57
6	1	−1	1	−1	42.1	41.43	0.67
7	−1	1	1	−1	69.3	72.88	−3.58
8	1	1	1	−1	51.2	51.25	−0.05
9	−1	−1	−1	1	49.6	51.22	−1.62
10	1	−1	−1	1	47.3	46.28	1.02
11	−1	1	−1	1	68.2	71.43	−3.23
12	1	1	−1	1	57.3	57.40	−0.10
13	−1	−1	1	1	42.5	43.25	−0.75
14	1	−1	1	1	56.9	56.22	0.68
15	−1	1	1	1	63.5	65.27	−1.77
16	1	1	1	1	67.3	69.13	−1.83
17	−2	0	0	0	91.6	85.92	5.68
18	2	0	0	0	57.9	59.35	−1.45
19	0	−2	0	0	54.9	55.92	−1.02
20	0	2	0	0	91.2	85.95	5.25
21	0	0	−2	0	35.9	33.65	2.25
22	0	0	2	0	36.9	34.92	1.98
23	0	0	0	−2	47.8	45.25	2.55
24	0	0	0	2	51.6	49.92	1.68
25	0	0	0	0	87.9	87.90	0.00
26	0	0	0	0	87.9	87.90	0.00
27	0	0	0	0	87.9	87.90	0.00
28	0	0	0	0	87.9	87.90	0.00
29	0	0	0	0	87.9	87.90	0.00
30	0	0	0	0	87.9	87.90	0.00

Table 3 ANOVA analysis for the obtained quadratic polynomial model

Source	Sum of squares	Degree of freedom	Mean square	F value	p value (Prob > F)	
model	10377.96	14	741.2829	86.82386	<0.0001	Significant
X_1	1058.682	1	1058.682	123.9997	<0.0001	
X_2	1353.002	1	1353.002	158.4723	<0.0001	
X_3	2.406667	1	2.406667	0.281884	0.6032	
X_4	32.66667	1	32.66667	3.826132	0.0693	
X_1X_2	82.81	1	82.81	9.699245	0.0071	
X_1X_3	320.41	1	320.41	37.5285	<0.0001	
X_1X_4	650.25	1	650.25	76.1615	<0.0001	
X_2X_3	3.24	1	3.24	0.37949	0.5471	
X_2X_4	9.61	1	9.61	1.125586	0.3055	
X_3X_4	6.25	1	6.25	0.732041	0.4057	
X_1^2	399.5505	1	399.5505	46.79795	<0.0001	
X_2^2	493.4876	1	493.4876	57.80048	<0.0001	
X_3^2	4928.138	1	4928.138	577.2155	<0.0001	
X_4^2	2786.458	1	2786.458	326.368	<0.0001	
Residual	128.07	15	8.54			
R^2	0.9878					
Adjusted R^2	0.9298					

Process optimization by CCD under RSM

30 experiments, with four factors and five levels for each factor were designed, listed in Table 2. Among these 30 experiments, six experiments were repetition of the central point (run No. 25–30). These are the experiments in which all of the factors are in the centric point of their values. The closeness of the responses of these six experiments can be a sign of the accuracy of the experiment process (Azami et al. 2012). For predicting the optimal values of MO discoloration within the experimental constrains, a second-order polynomial model was fitted to the experimental results for the MO discoloration ratio. The obtained polynomial model is shown as the following equation:

$$Y = 87.90 - 6.64X_1 + 7.51X_2 + 0.32X_3 + 1.17X_4 - 3.82X_1^2 - 4.42X_2^2 - 13.40X_3^2 - 10.08X_4^2 + 2.57X_1X_2 + 4.48X_1X_3 + 6.38X_1X_4 + 0.45X_2X_3 + 0.78X_2X_4 + 0.63X_3X_4 \quad (3)$$

Statistical testing of this model was implemented using analysis of variance (ANOVA), and the results for the coded variable levels are shown in Table 3. From ANOVA analysis, it can be known that the calculated F value is 86.82, much larger than the critical value of 2.42 for $F_{0.05}$ (14, 15), which implies that the derived quadratic polynomial model is significant (Sun and Lemley 2011). The low probability value (p<0.0001) means that there is only a 0.01 % chance that such model can occur due to noise (Rosales et al. 2012). The determination coefficient (R^2) quantitatively evaluates the correlation between the experimental data and the predicted responses (Fathinia et al. 2010). The experimental results and the predicted ones obtained from the model (Eq. 3)) are compared, as listed in Table 2. It can be found that the predicted values match the experimental ones reasonably well with R^2=0.9878 and adjusted R^2=0.9298. Figure 5 suggests that the predicted discoloration ratio of MO agrees well with the experimental values, indicating a high significance of the model (Karthikeyan et al. 2012). In addition, the values of Prob>F less than 0.0500 indicate model terms are

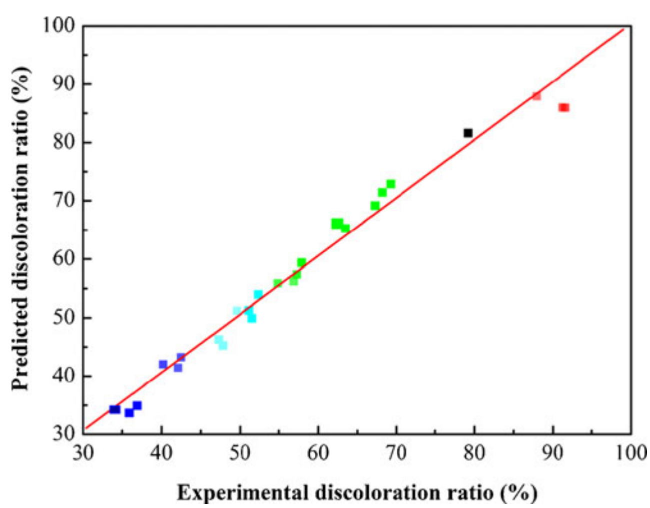

Fig. 5 Comparison of the predicted discoloration ratios and the experimental values

significant and values greater than 0.1000 indicate the model terms are not significant (Rosales et al. 2012). In this study, X_1, X_2, X_1X_3, X_1X_4, X_1^2, X_2^2, X_3^2 and X_4^2 are significant model terms are significant model terms. The Pareto analysis also gives more significant information for ANOVA analysis. The percentage effect of each factor on the response was introduced and calculated according to the following equation (Fathinia et al. 2010; Rosales et al. 2012):

$$P_i = \left(\frac{\beta_i^2}{\sum \beta_i^2} \right) \times 100 \quad (i \neq 0) \tag{4}$$

The Pareto graphic analysis of MO discoloration is illustrated in Fig. 6, where it can be seen that, among these variables, the linear effect of both MO initial concentration (X_1, 9.13 %) and reaction time (X_2, 11.68 %), the quadratic effect of all the four variables (X_1^2, 3.02; X_2^2, 3.72; X_3^2, 37.19 and X_4^2, 21.04) as well as the interactive effect of MO initial concentration and catalyst dosage (X_1X_3, 4.16 %) and MO initial concentration and solution pH (X_1X_4, 8.43 %) are significant in photocatalytic discoloration of MO. The results are in agreement with ANOVA analysis.

The influences of the four different variables on MO discoloration were visualized in 3D response surface plots (Fig. 7a–f), which show the interactive effects of two factors on MO discoloration. These findings reveal that the interactions between two independent variables are significant for MO discoloration, because the curvature of three-dimensional surfaces is obvious (Mohajeri et al. 2010; Lak et al. 2012). Furthermore, it can be observed from these figures that MO discoloration ratio increases with reaction time increasing and

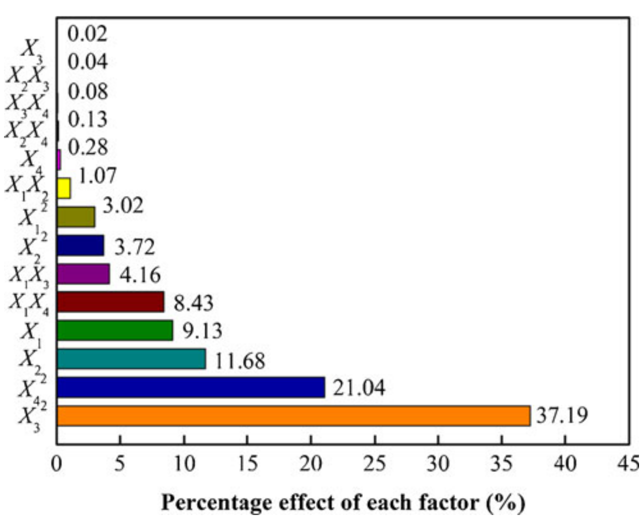

Fig. 6 Pareto graphic analyses for the photocatalytic discoloration of MO

MO initial concentration decreasing, while, there exist optimum values for photocatalyst dosage and solution pH. The slight decrease of photocatalytic discoloration efficiency with an increase in MO initial concentration might be attributed to several factors. Firstly, higher dye concentration made more adsorbed dye molecules occupy the active sites of TiO_2 surface. This suggested that as the dye concentration increased, more and more dye molecules would be adsorbed on the surface of the photocatalyst. Accordingly, generation of the reactive species (•OH and $•O_2^-$) needed for the degradation of the dye decreased; secondly, more intermediates would be generated at higher dye concentration, which could also be adsorbed on the surface of the solid catalyst. Slow diffusion of the generated intermediates from the catalyst surface could lead to the deactivation of the photocatalyst and consequently, a reduction in the degradation efficiency; thirdly, at higher dye concentration, more absorption of light photon by the dye itself resulted in a lesser availability of photons for reactive species generation (Fathinia et al. 2010). The interpretation of pH effects on the efficiency of dye photodegradation process was a very difficult task. Multiple roles of solution pH were involved in the ionization state of the surface of TiO_2, formation of the reactive species by the reaction between hydroxide ions and positive holes, agglomeration of TiO_2 particles under acidic conditions, and nature of a particular dye (Akpan and Hameed 2009). In this study, from pH 3 to 6.5, MO discoloration ratio, i.e., photocatalytic activity increased remarkably, then decreased dramatically from pH 6.5 to 11. The surface charge properties of TiO_2 changed with pH. The point of zero charge (pH_{PZC}) for titanium dioxide is at pH≈6.5. The TiO_2 surface is positively charged in acid solution ($pH<pH_{PZC}$) and negatively charged in alkaline solution ($pH>pH_{PZC}$) (Liu et al. 2007). At acidic pHs (3–6.5), the positively charged surface of TiO_2 facilitated the adsorption of MO, a anionic dye by the electrostatic attraction, which would be beneficial for the discoloration of MO. Moreover, with the solution pH increasing during this acidic range, agglomeration of TiO_2 particles could be overcome to produce more surface area and the amount of hydroxide ions in solution would increase, which would help to the generation of reactive species. Hence, photocatalytic activity increased remarkably from pH 3 to 6.5. Meanwhile, at alkaline pHs (6.5–11), the negatively charged surface of TiO_2 made MO dye molecules scarcely adsorbed due to the electrostatic repulsion, which resulted in the decrease of MO discoloration ratio during this basic pH range. It has been confirmed that there was a limit of catalyst dosage for the photodegradation of a particular pollutant in wastewater, above which the rate of photocatalysis would even decrease (Akpan and Hameed 2009). The similar phenomenon was observed in this study that below the optimum catalyst dosage, MO discoloration ratio increased with catalyst dosage increasing; while above this optimum dosage, the trend was opposite. The possible reason for this phenomenon might be attributed

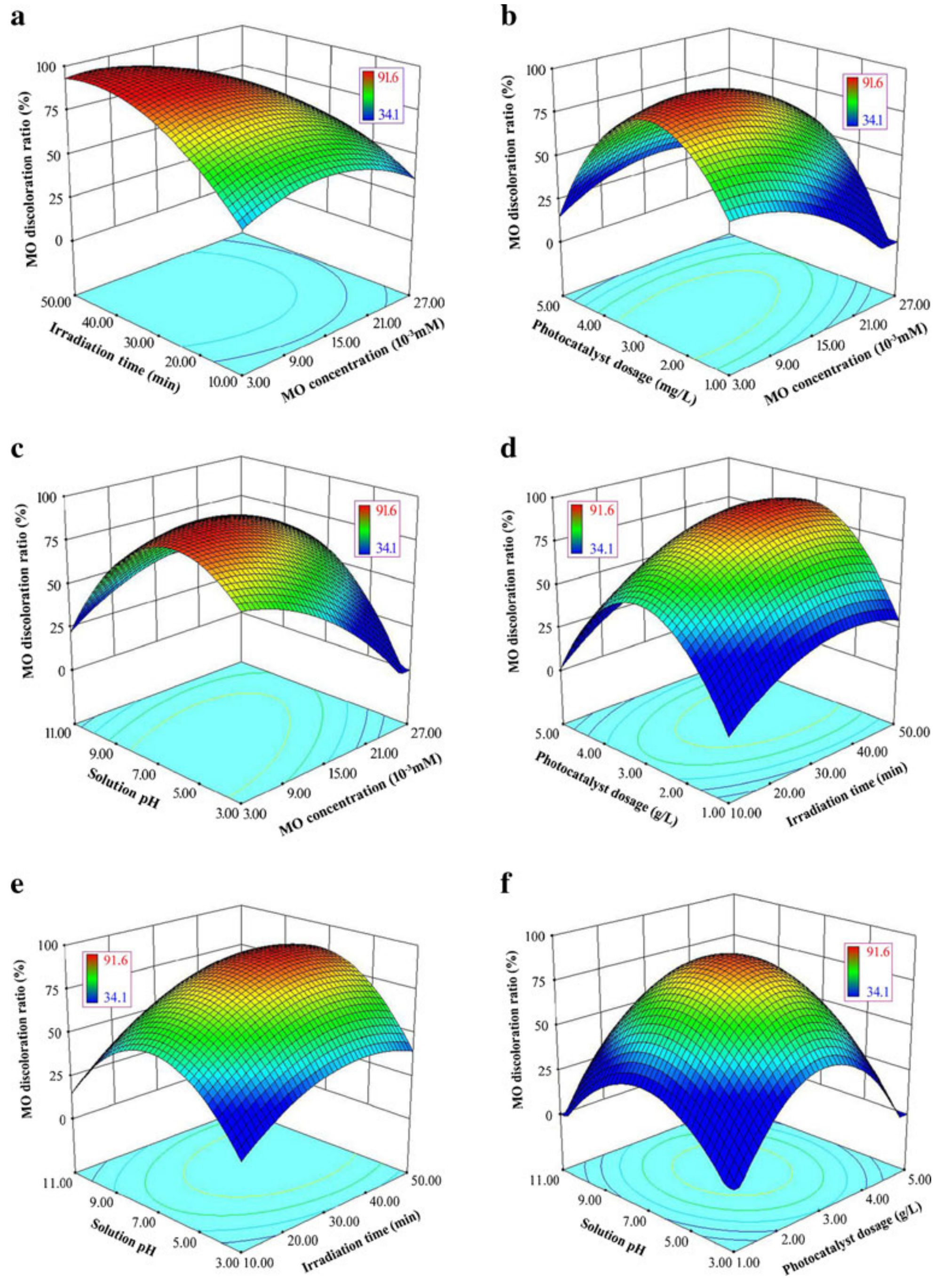

Fig. 7 The response surface plots for MO discoloration with different interactive effects of **a** MO initial concentration and reaction time; **b** MO initial concentration and photocatalyst dosage; **c** MO initial concentration and solution pH; **d** reaction time and photocatalyst dosage; **e** reaction time and solution pH; **f** photocatalyst dosage and solution pH

to the fact that, with catalyst dosage increasing below the optimum value, the active sites on the photocatalyst surface increased and accordingly reactive species increased; when the catalyst dosage increased above the optimum value, photocatalytic activity decreased due to the interception of the light photon by the higher concentration TiO_2 suspending particles.

Based on the model prediction, the optimum conditions for the photocatalytic discoloration of MO by TiO_2/schorl composite were determined to be 15×10^{-3} mM MO initial concentration, 2.7 g/l photocatalyst dosage, solution pH 6.6 and 43 min reaction time, with the maximum MO discoloration ratio of 98.6 %. Finally, a discoloration ratio of 94.3 % was achieved for the removal of MO from the real sample under the optimum conditions, which is very close to the predicted one. The standard deviation between the predicted and experimental values was calculated as 3.04 %, implying a validation of this process optimization. Hence, it has been confirmed that RSM is a powerful and satisfactory strategy to optimize the operational parameters for the photocatalytic discoloration of MO by anatase/schorl composite.

Conclusions

In this work, anatase/schorl composites were prepared by Sol–gel method and developed as good photocatalysts for the discoloration of MO under UV irradiation. XRD results indicated that TiO_2 existed in the form of anatase phase and no rutile phase could be found in all the composite samples, and no XRD diffraction peaks of schorl could be observed for all composite samples, which might be attributed to the fact that the content of schorl was so low that it could not be detected by XRD. SEM observations showed that the particles of TiO_2 were well deposited and dispersed on the surface of schorl. The photocatalytic experiments indicated that the MO discoloration ratio by TiO_2/schorl composite catalyst was much higher than that by the pure TiO_2, implying that schorl could improve the photocatalytic activity of TiO_2. When the pure TiO_2 was used as photocatalyst, only 45 % MO could be discolored within 60 min irradiation, whereas more than 90 % MO discoloration ratio could be obtained in the same reaction time for the sample with 3 wt.% content of schorl, which was determined to be the optimum photocatalyst in this study.

With the goal of the process optimization, 30 experiments, with four factors and five levels for each factor were designed by CCD under RSM. For predicting the optimal values of MO discoloration within the experimental constrains, a second-order polynomial model was fitted to the experimental results for the MO discoloration ratio. From ANOVA analysis, it could be known that the calculated F value was 86.82, much larger than the critical value of 2.42 for $F_{0.05}$ (14, 15), which implied that the derived quadratic polynomial model was significant. The predicted discoloration ratio of MO agreed well with the experimental values with R^2=0.9878 and adjusted R^2=0.9298, also indicating a high significance of the model. The Pareto graphic analysis showed that, among these variables, the linear effect of both MO initial concentration (X_1, 9.13 %) and reaction time (X_2, 11.68 %), the quadratic effect of all the four variables (X_1^2, 3.02; X_2^2, 3.72; X_3^2, 37.19 and X_4^2, 21.04) as well as the interactive effect of MO initial concentration and catalyst dosage (X_1X_3, 4.16 %) and MO initial concentration and solution pH (X_1X_4, 8.43 %) were significant in photocatalytic discoloration of MO. Finally, based on the model prediction, the optimum conditions for the photocatalytic discoloration of MO by anatase/schorl composite were determined to be 15×10^{-3} mM MO initial concentration, 2.7 g/l photocatalyst dosage, solution pH 6.6 and 43 min reaction time, with the maximum MO discoloration ratio of 98.6 %. A discoloration ratio of 94.3 % was achieved for the removal of MO from the real sample under the optimum conditions, which is very close to the predicted one.

Acknowledgement This work was supported by National Natural Science Foundation of China (No. 51002040), National College Students' Innovative Training Project (No. 201210214006) and Science Foundation of the Heilongjiang Education Office (No. 12521071). Furthermore, Program for New Century Excellent Talents in Heilongjiang Provincial Universities (1253-NCET-010), Reserve Talents of Universities Overseas Research Program of Heilongjiang and Young Outstanding Talents Project of Harbin University of Science and Technology were also appreciated by Huan-Yan Xu.

References

Akpan UG, Hameed BH (2009) Parameters affecting the photocatalytic degradation of dyes using TiO_2-based photocatalysts: a review. J Hazard Mater 170:520–529

Arslan-Alaton I, Yalabik AB, Olmez-Hanci T (2010) Development of experimental design models to predict photo-Fenton oxidation of a commercially important naphthalene sulfonate and its organic carbon content. Chem Eng J 165:597–606

Azami M, Bahram M, Nouri S, Naseri A (2012) A central composite design for the optimization of the removal of the azo dye, methyl orange, from waste water using the Fenton reaction. J Serb Chem Soc 77:235–246

Baek M-H, Yoon J-W, Hong J-S, Suh J-K (2013a) Application of TiO_2-containing mesoporous spherical activated carbon in a fluidized bed photoreactor: adsorption and photocatalytic activity. Appl Catal A Gen 450:222–229

Baek M-H, Jung W-C, Yoon J-W, Hong J-S, Lee Y-S, Suh J-K (2013b) Preparation, characterization and photocatalytic activity evaluation of micro- and mesoporous TiO_2/spherical activated carbon. J Ind Eng Chem 19:469–477

Bian X, Chen J, Ji R (2013) Degradation of 2,4-dichlorophenoxyacetic acid (2,4-D) by novel photocatalytic material of tourmaline-coated TiO_2 nanoparticles: kinetic study and model. Materials 6:1530–1542

Blain P, Wayde NM, Ray LF (2012) Immobilised anatase on clay mineral particles as a photocatalyst for herbicides degradation. Appl Clay Sci 57:49–54

Chen L, Deng C, Wu F, Deng N (2011) Decolorization of the azo dye Orange II in a montmorillonite/H_2O_2 system. Desalination 281:306–311

Chen D, Zhu Q, Zhou F, Deng X, Li F (2012) Synthesis and photocatalytic performances of the TiO_2 pillared montmorillonite. J Hazard Mater 235–236:186–193

Coleman HM, Chiang K, Amal R (2005) Effects of Ag and Pt on photocatalytic degradation of endocrine disrupting chemicals in water. Chem Eng J 113:65–72

Da Dalt S, Alves AK, Bergmann CP (2013) Photocatalytic degradation of methyl orange dye in water solutions in the presence of MWCNT/TiO_2 composites. Mater Res Bull 48:1845–1850

Dong W, Sun Y, Ma Q, Zhu L, Hua W, Lu X, Zhuang G, Zhang S, Guo Z, Zhao D (2012) Excellent photocatalytic degradation activities of ordered mesoporous anatase TiO_2–SiO_2 nanocomposites to various organic contaminants. J Hazard Mater 229:307–320

Eliyas AE, Ljutzkanov L, Stambolova ID, Blaskov VN, Vassilev SV, Razkazova-Velkova EN, Mehandjiev DR (2013) Visible light photocatalytic activity of TiO_2 deposited on activated carbon. Cent Eur J Chem 11:464–470

Fathinia M, Khataee AR, Zarei M, Aber S (2010) Comparative photocatalytic degradation of two dyes on immobilized TiO_2 nanoparticles: effect of dye molecular structure and response surface approach. J Mol Catal A: Chem 333:73–84

Gilpavas E, Dobrosz-Gómez I, Gómez-García MÁ (2012) Decolorization and mineralization of Diarylide Yellow 12 (PY12) by photo-Fenton process: the Response Surface Methodology as the optimization tool. Water Sci Technol 65:1795–1800

Harraz FA, Abdel-Salam OE, Mostafa AA, Mohamed RM (2013) Rapid synthesis of titania–silica nanoparticles photocatalyst by a modified sol–gel method for cyanide degradation and heavy metals removal. J Alloys Compd 551:1–7

Huang D, Xie W, Tu Z, Zhang F, Quan S, Liu L (2013) N-TiO_2/gamma-Al_2O_3 granules: preparation, characterization and photocatalytic activity for the degradation of 2,4-dichlorophenol. J Nanosci Nanotechnol 13:260–269

Juang L-C, Semblante GU, You S-J, Hong S-H (2013) Degradation of 2-chlorophenol using carbon nanotube/titanium oxide composite prepared by hydrothermal method. J Taiwan Inst Chem E 44:432–437

Kamegawa T, Kido R, Yamahana D, Yamashita H (2013) Design of TiO_2–zeolite composites with enhanced photocatalytic performances under irradiation of UV and visible light. Micropor Mesopor Mat 165:142–147

Karthikeyan S, Gupta VK, Boopathy R, Titus A, Sekaran G (2012) A new approach for the degradation of high concentration of aromatic amine by heterocatalytic Fenton oxidation: kinetic and spectroscopic studies. J Mol Liq 173:153–163

Khataee AR, Safarpour M, Zarei M, Aber S (2012) Combined heterogeneous and homogeneous photodegradation of a dye using immobilized TiO_2 nanophotocatalyst and modified graphite electrode with carbon nanotubes. J Mol Catal A Chem 363–364:58–68

Kibanova D, Sleiman M, Cervini-Silva J, Destaillats H (2012) Adsorption and photocatalytic oxidation of formaldehyde on a clay–TiO_2 composite. J Hazard Mater 211–212:233–239

Lak MG, Sabour MR, Amiri A, Rabbani O (2012) Application of quadratic regression model for Fenton treatment of municipal landfill leachate. Waste Manage 32:1895–1902

Li W, Liu S (2012) Bifunctional activated carbon with dual photocatalysis and adsorption capabilities for efficient phenol removal. Adsorption 18:67–74

Li J, Zhou SL, Hong G-B, Chang C-T (2013) Hydrothermal preparation of P25–graphene composite with enhanced adsorption and photocatalytic degradation of dyes. Chem Eng J 219:486–491

Lin C, Song Y, Cao L, Chen S (2013) Effective photocatalysis of functional nanocomposites based on carbon and TiO_2 nanoparticles. Nanoscale 5:4986–4992

Liu SX, Chen XY, Chen X (2007) A TiO_2/AC composite photocatalyst with high activity and easy separation prepared by a hydrothermal method. J Hazard Mater 143:257–263

Meng J-P, Liang J-S, Liang G-C, Yu J-M, Pan Y-F (2006) Effects of tourmaline on microstructures and photocatalytic activity of TiO_2/SiO_2 composite powders. Trans Nonferrous Metals Soc China 16:s547–s550

Mohajeri S, Aziz HA, Isa MH, Zahed MA, Adlan MN (2010) Statistical optimization of process parameters for landfill leachate treatment using electro-Fenton technique. J Hazard Mater 176:749–758

Mohamed RM, Baeissa ES (2013) Mordenite encapsulated with Pt-TiO_2: characterization and applications for photocatalytic degradation of direct blue dye. J Alloys Compd 558:68–72

Mohanta O, Singhbabu YN, Giri SK, Dadhich D, Das NN, Sahu RK (2013) Degradation of Congo red pollutants using microwave derived $SrFe_{12}O_{19}$: an efficient magnetic photocatalyst under visible light. J Alloys Compd 564:78–83

Morales-Torres S, Pastrana-Martinez LM, Figueiredo JL, Faria JL, Silva AMT (2013) Graphene oxide-P25 photocatalysts for degradation of diphenhydramine pharmaceutical and methyl orange dye. Appl Surf Sci 275:361–368

Nakamura T, Kubo T (1992) Tourmaline group crystals reaction with water. Ferroelectrics 137:13–31

Ong S-A, Ho L-N, Wong Y-S, Raman K, Bahari R (2013) Mineralization of Methyl Orange-containing wastewater by integrated anaerobic and aerobic processes using spent granular activated carbon-biofilm under sequencing batch reactor operation. Desalin Water Treat 51:2813–2819

Papoulis D, Komarneni S, Panagiotaras D, Stathatos E, Toli D, Christoforidis KC, Fernandez-Garcia M, Li H, Yin S, Sato T, Katsuki H (2013) Halloysite–TiO_2 nanocomposites: synthesis, characterization and photocatalytic activity. Appl Catal B Environ 132–133:416–422

Petrella A, Petrella M, Boghetich G, Mastrorilli P, Petruzzelli V, Ranieri E, Petruzzelli D (2013) Laboratory scale unit for photocatalytic removal of organic micropollutants from water and wastewater: Methyl Orange degradation. Ind Eng Chem Res 52:2201–2208

Ramírez C, Saldaña A, Hernández B, Acero R, Guerra R, Garcia-Segura S, Brillas E, Peralta-Hernández JM (2013) Electrochemical oxidation of methyl orange azo dye at pilot flow plant using BDD technology. J Ind Eng Chem 19:571–579

Rosales E, Sanromán MA, Pazos M (2012) Application of central composite face-centered design and response surface methodology for the optimization of electro-Fenton decolorization of Azure B dye. Environ Sci Pollut Res 19:1738–1746

Sedneva TA, Belikov ML, Lokshin EP (2013) Ferroin adsorption and decomposition on TiO_2/Al_2O_3 photocatalytic nanocomposites. Inorg Mater 49:468–476

Song SH, Kang M (2008) Decomposition of 2-chlorophenol using a tourmaline photocatalytic system. J Ind Eng Chem 14:785–791

Su Y, Zhang X, Zhou M, Han S, Lei L (2008) Preparation of high efficient photoelectrode of N-F-codoped TiO_2 nanotubes. J Photochem Photobiol A Chem 194:152–160

Sun SP, Lemley AT (2011) *p*-Nitrophenol degradation by a heterogeneous Fenton-like reaction on nano-magnetite: process optimization, kinetics, and degradation pathways. J Mol Catal A Chem 349:71–79

Torkian L, Amini MM, Amereh E (2013) Sol–gel synthesised silver doped TiO_2 nanoparticles supported on NaX zeolite for photocatalytic applications. Mater Technol 28:111–116

Umar M, Aziz HA, Yusoff MS (2010) Trends in the use of Fenton, electro-Fenton and photo-Fenton for the treatment of landfill leachate. Waste Manage 30:2113–2121

Wang P, Wang J, Wang X, Yu H, Yu J, Lei M, Wang Y (2013) One-step synthesis of easy-recycling TiO_2–rGO nanocomposite photocatalysts with enhanced photocatalytic activity. Appl Catal B Environ 132:452–459

Wei W, Yu C, Zhao Q, Li G, Wan Y (2013) Improvement of the visible-light photocatalytic performance of TiO_2 by carbon mesostructures. Chem Eur J 19:566–577

Xie B, Xiong Y, Chen R, Chen J, Cai P (2005) Catalytic activities of Pd-TiO_2 film towards the oxidation of formic acid. Catal Commun 6:699–704

Xu H-Y, Zheng Z, Mao G-J (2010) Enhanced photocatalytic discoloration of acid fuchsine wastewater by TiO_2/schorl composite catalyst. J Hazard Mater 175:658–665

Xu H, Zhang Y, Jiang Q, Reddy N, Yang Y (2013) Biodegradable hollow zein nanoparticles for removal of reactive dyes from wastewater. J Environ Manage 125:33–40

Yoon J-W, Baek M-H, Hong J-S, Lee C-Y, Suh J-K (2012) Photocatalytic degradation of azo dye using TiO_2 supported on spherical activated carbon. Korean J Chem Eng 29:1722–1729

Zendehzaban M, Sharifnia S, Hosseini SN (2013) Photocatalytic degradation of ammonia by light expanded clay aggregate (LECA)-coating of TiO_2 nanoparticles. Korean J Chem Eng 30:574–579

Zhang A, Fang L, Wang J, Liu W (2013a) Enzymatic decolorization of Orange II: optimization by response surface methodology and pathway. Environ Prog Sustain Energy 32:294–301

Zhang W, Bi F, Yu Y, He H (2013b) Phosphoric acid treating of ZSM-5 zeolite for the enhanced photocatalytic activity of TiO_2/HZSM-5. J Mol Catal A Chem 372:6–12

Zhao D, Yang X, Chen C, Wang X (2013) Enhanced photocatalytic degradation of methylene blue on multiwalled carbon nanotubes-TiO_2. J Colloid Interf Sci 398:234–239

Zhou W, Zhou Y, Tang S (2005) Formation of TiO_2 nano-fiber doped with Gd^{3+} and its photocatalytic activity. Mater Lett 59:3115–3118